An Experimental Method Dedicated to the Dynamic Characterization of Structural Adhesives under Drop Weight Conditions

Benjamin Valès, Steven Marguet, Romain Créac'Hcadec, Laurent Sohier, Jean-François Ferrero, Pablo Navarro

An Experimental Method Dedicated to the Dynamic Characterization of Structural Adhesives under Drop Weight Conditions

B. Valès[a], S. Marguet[a,*], R. Créac'hcadec[b], L. Sohier[c], J.-F. Ferrero[a], P. Navarro[a]

[a]*Université de Toulouse, Institut Clément Ader (ICA), UMR CNRS 5312, UPS/INSA/ISAE/Mines Albi, 3 rue Caroline Aigle, F-31400 Toulouse, France*
[b]*ENSTA Bretagne, Institut de Recherche Dupuy de Lôme (IRDL), UMR CNRS 6027, 29806 Brest, France*
[c]*Université de Bretagne Occidentale, Institut de Recherche Dupuy de Lôme (IRDL), UMR CNRS 6027, 29200 Brest, France*

Abstract

Adhesive bonding is a commonly used method in multi-materials assemblies dedicated to the transport fields. In order to ensure structures integrity and users safety, the knowledge of the mechanical behaviour of structural adhesives used in these assemblies under impact conditions appears to be an essential prerequisite. To date, numerous tests combining usual specimens geometry *e.g.* single lap joint, butt joint, *etc.* and high velocity testing rigs exist and are used. Among these, most allow comparative studies and a few provide a partial identification of the material properties of the investigated adhesive.

In this study, an experimental method dedicated to the dynamic characterization of structural adhesives under drop weight condition is proposed. On the basis of existing works, a modified Arcan specimen and a dynamic tensile testing mean were developed and are presented. The Arcan geometry allows to test the adhesive under various loading directions and so to obtain its mechanical response envelope. Design strategies are also implemented in order to obtain time stable and quasi-homogeneous stress distributions in the adhesive during the tests.

At last, the dynamic characterization of a Dow® Betamate™ 1496V adhesive is proposed. Results are repeatable and show a strain rate dependent behaviour validating the appropriateness of the experimental approach.

Keywords: Modified Arcan device, [C.] Dynamic mechanical analysis, [D.] Mechanical properties of adhesives, [D.] Impact

1. Introduction

Over the past two decades, there has been a growing interest in the study of the dynamic behaviour of structural adhesives. This is partly due to the fact that most of the modern structures from transport industry become complex assemblies designed with the aim to be light. These are then generally composed of parts made with different materials, of complex geometry, *etc.* which can be only well assembled by adhesive bonding process.

* *Corresponding author
Email address: steven.marguet@univ-tlse3.fr (S. Marguet)

Adhesives being polymeric materials, it is well known that their mechanical properties are, in general, strain rate dependant. Therefore, it is hence necessary to characterize their dynamic mechanical behaviour in order to implement calculation models and to ensure users safety. The study of impact on helicopter blade proposed by Tawk in [1] is a good illustration of this problematic.

With strain rate increases, the adhesives usually tend to react with higher stress and lesser ductility, which cause higher resisting loads but lower absorbed energy. That is the mean reason why the common first and only standard impact tests ASTM D950 Block Impact Test [2] and ISO 11343 Wedge Impact Peel Test [3] developed between the 70's and the 90's aim at measuring the energy required to create the failure of the specimen. Besides the critical assessment of the ASTM D950 test by Adams and Harris in [4], these "energy" oriented tests are interesting for comparative studies but do not allow to extract material properties which can be used for numerical purposes for example.

Since then, numerous dynamic tests have been developed with different specimen geometries and test rigs. Typically, single lap joint [5], butt joint [6] and bulk samples [7] are the most studied specimens under dynamic loadings because they are well known and commonly used under quasistatic assumptions. Nevertheless, these conventional geometries are specific and allow generally to test the adhesive following a single loading direction (*e.g.* single lap joint is a "shear" test). Testing means allowing to set in motion these specimens at high velocity rates generally correspond to servo hydraulic systems, Izod and Charpy pendulums, split Hopkinson pressure bar (SHPB) techniques, drop weight tower and powder & gas gun. Test rig choice is mainly based on the desired strain rates [8, 9, 10] corresponding to a related phenomenon *i.e.* automobile crash, aircraft impact *etc.* Goglio in [11], da Silva *et al.* in [12] and Sato in [8] provide excellent reviews of these experimental test methods.

Works presented in this paper deal with the use of a modified Arcan specimen under drop weight assumptions for structural adhesive characterization purposes. Specimen and test rig choices are based on previous in depth numerical [13] and experimental [14] studies conducted on the evaluation of the use of the Tensile/Compression-Shear (TCS) Arcan specimen developed by Créac'hcadec *et al.* [15] for quasistatic purposes under drop weight conditions. The Arcan TCS combines two interesting technological aspects: (1) its global geometry based on the work of Arcan *et al.* [16] allows to test the adhesive joint under different loading directions; (2) its local geometry near the adhesive layer, inspired by the work of Cognard *et al.* [17, 18], limits stress singularities in the adhesive well known as "edge effects". The drop weight tower allows to vary independently and over a wide ranges of values the velocity and the energy of the impact via the falling height/impactor mass couple. Furthermore, strain rates values, which can be obtained in the adhesive with this test rig *i.e.* between 10^2 and $10^4 s^{-1}$, are representative of most applications from the transport industry [8]. Main results from these studies combining the Arcan TCS and a drop weight show that: (1) it is possible to extract numerous, reliable and relevant data from the specimen at high strain rates; (2) the mass of the impactor has a significant influence on the ability to produce a time and spatial stable loading of the adhesive.

From these two studies and associated conclusions, a specimen and a testing mean dedicated to the characterization of structural adhesives under high strain rate were developed and are the subject of this paper. In a first part, a global description of the modified Arcan specimen is made. Then, the developed dynamic tensile testing device and post processing methods used to strip tests are described. At last, results associated to the dynamic

characterization of a Dow® Betamate™ 1496V adhesive are presented. These ones are numerous, reliable and repeatable and show a non-linear and strain rate dependent mechanical behaviour.

2. Modified Arcan specimen

The specimen used for this study and shown in Fig. 1a corresponds to an evolution of the Arcan Tensile/Compression-Shear (TCS) specimen developed by Créac'hcadec *et al.* [15] studied under dynamic assumptions in [14]. This easy to implement and reusable device allows to extract the mechanical response envelope of an adhesive while minimizing the edge effects occurring near the free ends of the joint.

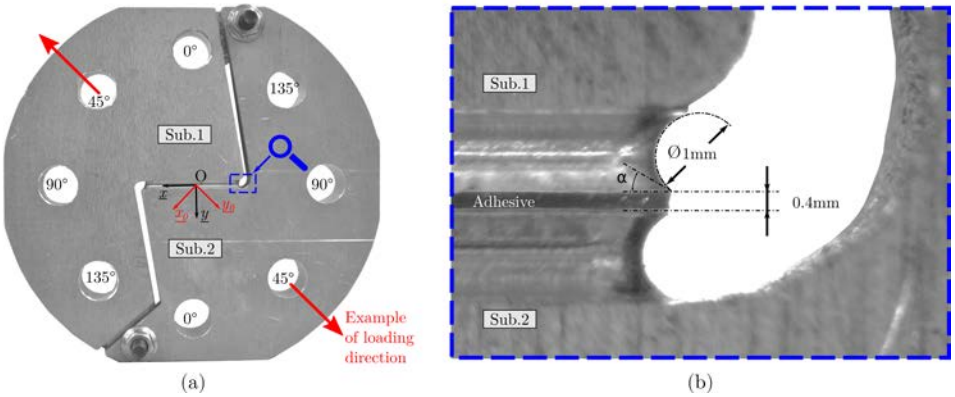

Figure 1: Modified Arcan specimen. (a) General view of the test specimen. (b) Zoom on the local geometry of the beaks.

This assembly is composed of two metal substrates ("Sub.1" and "Sub.2") linked by an adhesive seal measuring 25 (length)×10 (width)×0.4 mm (thickness). For the remainder of the study, two orthonormal coordinate systems are used: (1) $\left(O, \underline{x_0}, \underline{y_0}\right)$ is associated to the test rig $\underline{y_0}$ where is oriented along the axial loading direction; (2) $\left(O, \underline{x}, \underline{y}\right)$ is attached to the test specimen and aligned with the adhesive. $\underline{y}$ corresponds to the thickness direction while $\underline{x}$ relates to the overlap direction.

The Arcan geometry is obtained by machining four holes on each substrate and allows to test the adhesive under various loading cases. Boundary conditions are applied on two opposite holes defined by their orientation compared with the normal of the lap joint $\underline{y}$ designated $\gamma = \left(\underline{y_0}, \underline{y}\right)$. Thus, if $\gamma = 0°$ (resp. 45°, 90° and 135°), *i.e.* the mechanical loading is applied on the holes noted 0°in Fig. 1a (resp. 45°, 90° and 135°), the loading case is a tensile test (resp. a tensile-shear test, a shear test and a compression-shear test).

Major changes on this specimen in comparison with the TCS one [14, 15] concern some aspects of the substrate geometry and the substrate material grade which enable to: (1) have a specimen designed for the load levels reached in dynamic and (2) to ensure a quasi-homogeneous stress distribution along the adhesive joint without edge effects. For the latter, two strategies are then implemented: (2.1) the use of a low ratio $\beta = E_s/E_a$ corresponding to the ratio between the Young's moduli of the substrates and the adhesive; (2.2) the use of two filleted cylindrical beaks of 1 mm diameter, which form an angle $\alpha = 30°$ with the lap joint (see the zoom Fig. 1b).

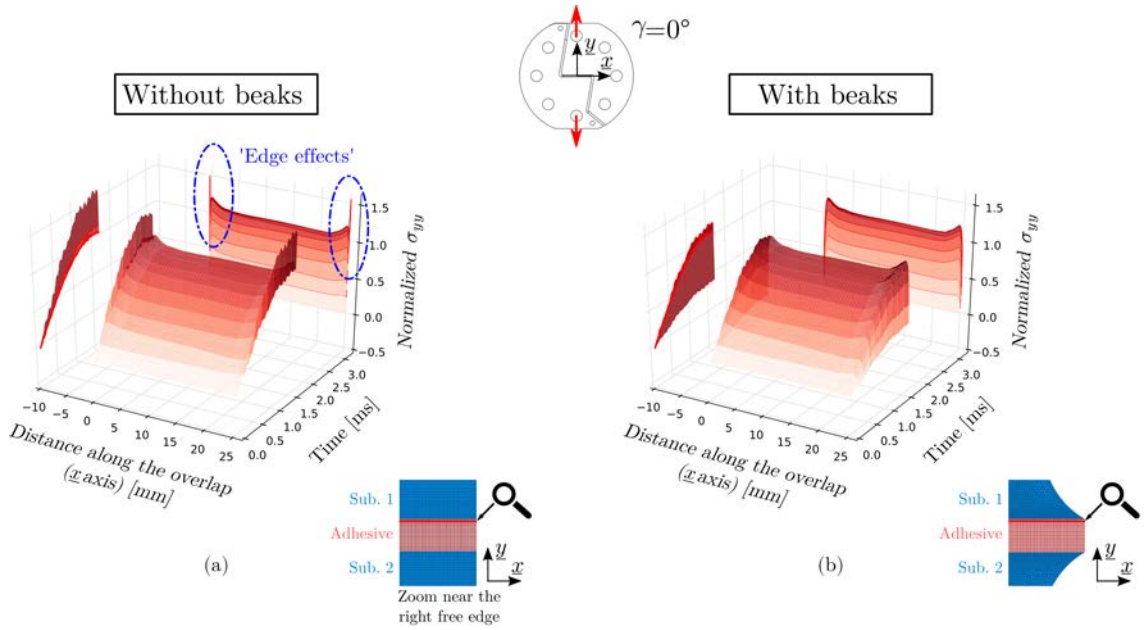

Figure 2: Spatial *vs*. temporal σ_{yy} distribution in the adhesive (near the substrate/adhesive interface) in the case of a tensile test. (a) Without the beaks. (b) With the beaks near the free edges.

The contribution of the local geometry near the free edges on the loading quality of the adhesive is shown on the Finite Element Analysis (FEA) results presented in Fig. 2.

A numerical model of the modified Arcan specimen is developed under the plane-stress assumption such as in [15], within the finite element software Abaqus. The time integration is performed by an explicit scheme. The joint is meshed with plane-stress, reduced integration quadrangular elements (16 elements along the thickness) while the substrates are meshed with plane-stress, reduced integration triangular elements. Rigid body relationships are introduced between half of the nodes of the upper and lower holes and their respective centres (master nodes) to introduce the boundary conditions. The two master nodes are free to rotate. The lower one is fixed in translation whereas the upper one is associated to a concentrated mass on which is imposed an initial velocity along a vertical slider.

The spatial *vs.* temporal normal stress component σ_{yy} distribution in the adhesive (near the substrate/adhesive interface, where the edge effects are greater) is plotted for two local geometries: a "no beaks" specimen in Fig. 2a and a "with beaks" specimen in Fig. 2b. These results are extracted from a tensile configuration with the same Finite Element Model (FEM) assumptions. The comparison of these two results clearly highlights the appropriateness of the use of beaks to mitigate the edge effects.

At last, the relative positioning of the two substrates during the manufacturing is done by using two shoulder screws which allow to control the thickness of the adhesive. Also, these latter protect the adhesive from unwanted loading during the handling of the specimen.

3. Dynamic tensile testing device

3.1. Global description

In order to investigate the influence of the strain rate on the mechanical behaviour of the adhesive, it is necessary to use a test rig which allows to respect two main specifications: (1) get the failure of the specimen on the first wave front and (2) ensure the loading monotony. These two specifications are complementary and are needed to get a qualitatively efficient test in terms of adhesive loading.

It was shown in [14] that under drop weight conditions, the use of a heavy impactor is one of the essential requirements needed to ensure the loading monotony of the adhesive. This can be shown through the results coming from FEA presented in Fig. 3. The spatial *vs.* temporal distribution of $-\sigma_{yy}$ in the mid plane of the adhesive of the specimen presented in section 2 is plotted for two impactor masses: a light one of 2 kg (see Fig. 3a) and a heavier one of 200 kg (see Fig. 3b). These results are extracted from a compression-shear configuration (the most affected by unwanted vibrations) with the same finite element model in both cases. The stress field obtained with the light mass exhibits harmful oscillations and an inhomogeneous stress distribution along the overlap through time. These last are linked to the excitation of harmonic modes of vibrations [13, 14]. By increasing the mass of the falling weight by a factor 100, results plotted in Fig. 3b show the ability of a heavy impactor to produce a time and spatial stable loading of the adhesive during the test.

From these observations, an original Dynamic Tensile Testing Device (DTTD) presented in Fig. 4 has been developed. It combines technological solutions from the test rig of Beevers

& Ellis [19] and from Split Hopkinson Pressure Bar (SPHB) testing means [12]. As it is shown in Fig. 4a, the DTTD is positioned under a drop weight tower and transform the kinetic energy stored by the falling mass in a tensile loading.

The device is composed of a chassis (in red in Fig. 4a) linked to the ground on which the Arcan specimen is iso-statically fixed in the top. The lower substrate of the specimen is connected to a rod of 2.5 m length placed below. In its lower end a end stop is fixed. It corresponds to the impacted part of the mounting. The impactor is guided by the drop weight tower and is therefore never in contact with the tensile rod.

The test is conducted as follows: (1) the lower surface of the impactor (falling mass) is raised to a distance h from the upper surface of the end stop; (2) it is then released and falls along the tensile rod under the gravity effect; (3) the falling mass impacts the end stop; (4) the shock wave propagates along the tensile rod and loads the specimen.

In order to extract relevant and reliable data from this test, the device is instrumented with: (1) a 50 kN U9C HBM© load sensor, with a natural mechanical frequency of 7.2 kHz and fixed above the test specimen (see Figs. 4d & e). This sensor relies on strain gauges technology (grid size 3 mm). As a result, its response time is similar to that of usual gauges.

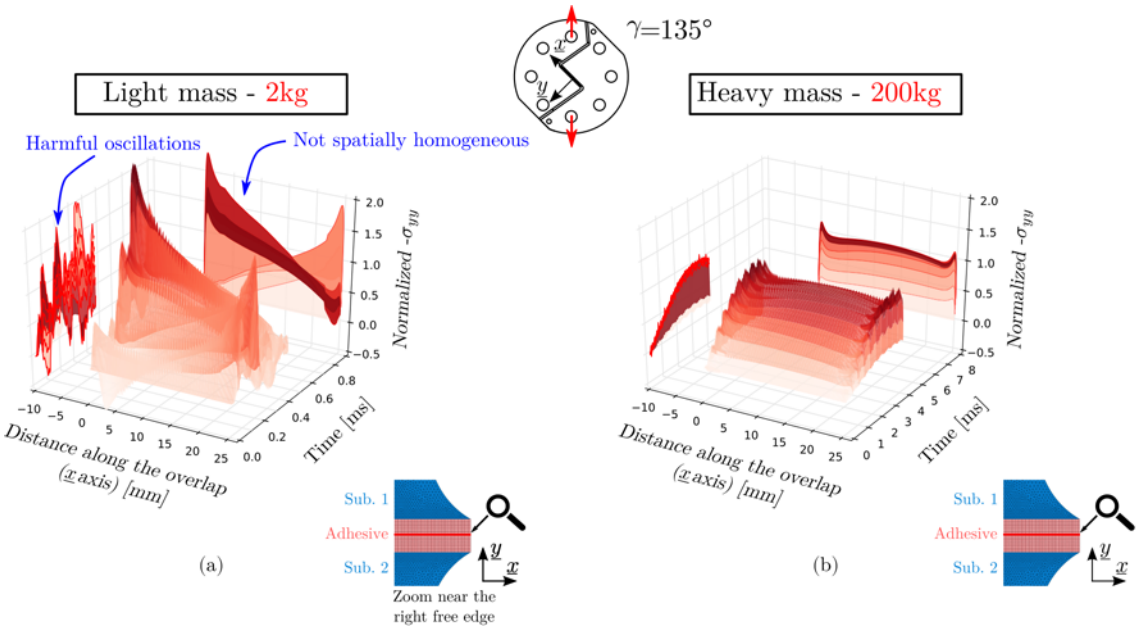

Figure 3: Spatial *vs.* temporal σ_{yy} distribution in the mid plane of the adhesive in the case of a compression-shear test. (a) With a light impactor of $m = 2$ kg. (b) With a heavy impactor of $m = 200$ kg.

The signal is recorded at the frequency of 1 MHz and filtered at 50 kHz; (2) two strain gauges named G_1 and G_2 glued on the tensile rod in opposition and along the loading direction $\underline{y_0}$ (see Figs. 4b & c); (3) a Photron© FASTCAM SA4 high-speed camera filming with a 192×128 px. resolution @ 100 kHz (see Fig. 4e).

One of the advantages of the DTTD is its loading modularity. Thus, it is possible to impact the end stop with an input velocity from $v \approx 0.1$ m.s^{-1} to $v \approx 5.5$ m.s^{-1} with an impactor mass greater than 100 kg allowing to have a wide range of input energy (from $\approx 5.10^{-1}$ J to $\approx 5.10^{3}$ J).

The material and geometry choices for the tensile rod were carried out in order to respect the two main specifications enunciated at the beginning of this section. To do this, a mass/spring system was studied by a finite element method. The model is composed of two springs in series modelled by truss elements which respectively represent the tensile rod and the specimen. For boundary conditions, the upper node of the "specimen" is clamped and its lower node is the same as the upper one of the rod. A concentrated mass is attached to the lower node of the rod (standing for the "end stop") and an initial velocity is imposed on it. Results from this FEA allowed to find: (1) the rod length required to avoid wave returns before the failure of the adhesive and (2) the rod stiffness which allows to obtain the failure on the first wave front (whatever the loading case and specimen orientation γ).

3.2. Examples of input loading signals

Some examples of experimental input loading signals are plotted in Fig. 5. They are extracted from the dynamic characterization of an Araldite® 420 A/B adhesive under tensile ((a) & (c)) and shear ((b) & (d)) loadings with an impactor mass $m = 200$ kg and a falling height $h = 0.5$ m.

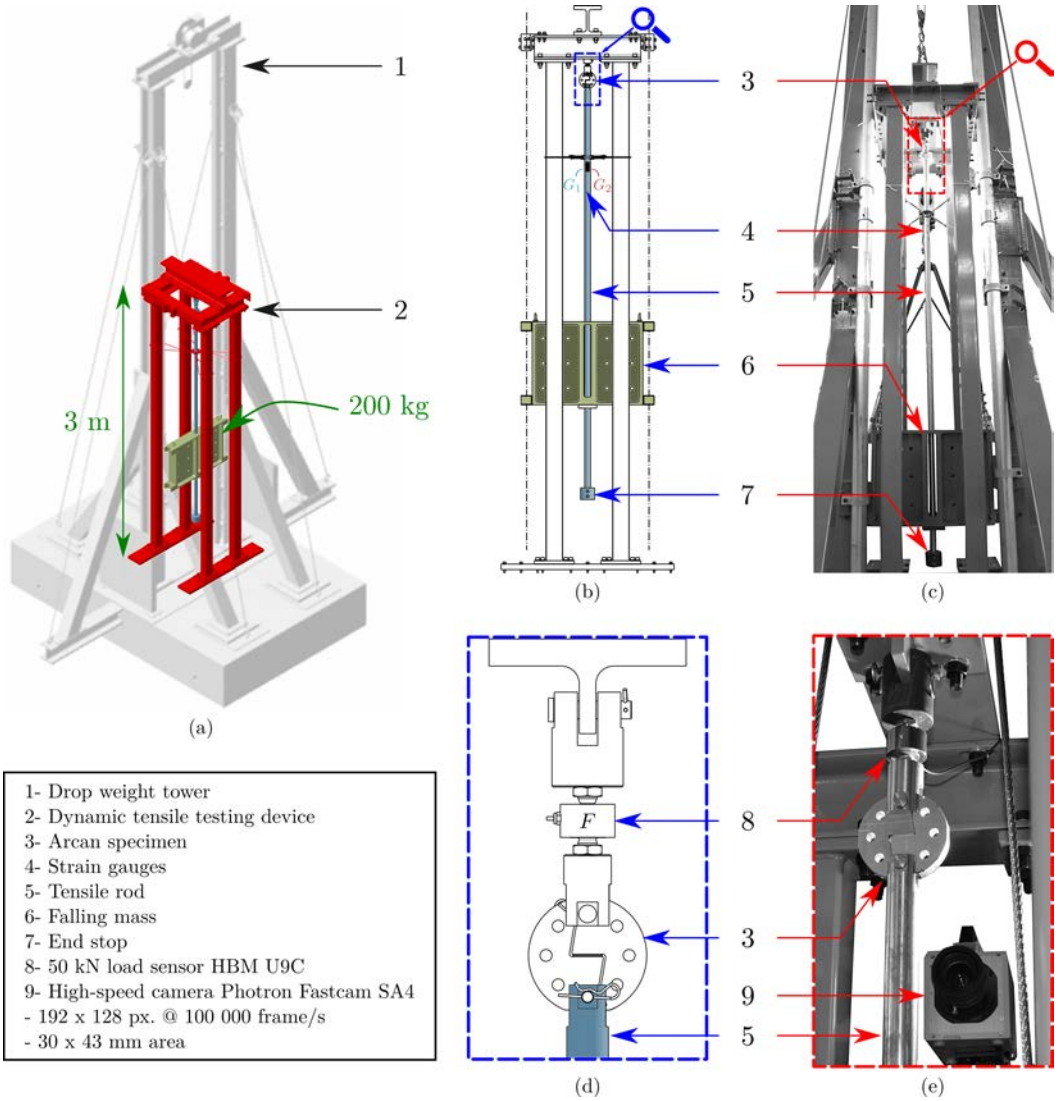

Figure 4: Dynamic Tensile Testing Device (DTTD). (a) DTTD integration under the drop weight tower. (b) Schema and (c) photo of the DTTD. (d) Schema and (e) photo of the acquisition system.

G_1 and G_2 strain gauges signals (see Figs. 4b & c for the location) are plotted respectively in blue and red dotted lines in Figs. 5a & b. The averages $\overline{G} = \frac{1}{2}(G_1 + G_2)$ signals are plotted in green full lines in Figs. 5a-d. Strain gauges signals magnitude G are given in Newton and are calculated as follows: $G = ES\varepsilon_{\underline{y0}}$, where $\varepsilon_{\underline{y0}}$, E and S correspond respectively to the strain measured by the gauges, the Young modulus and the section of the tensile rod.

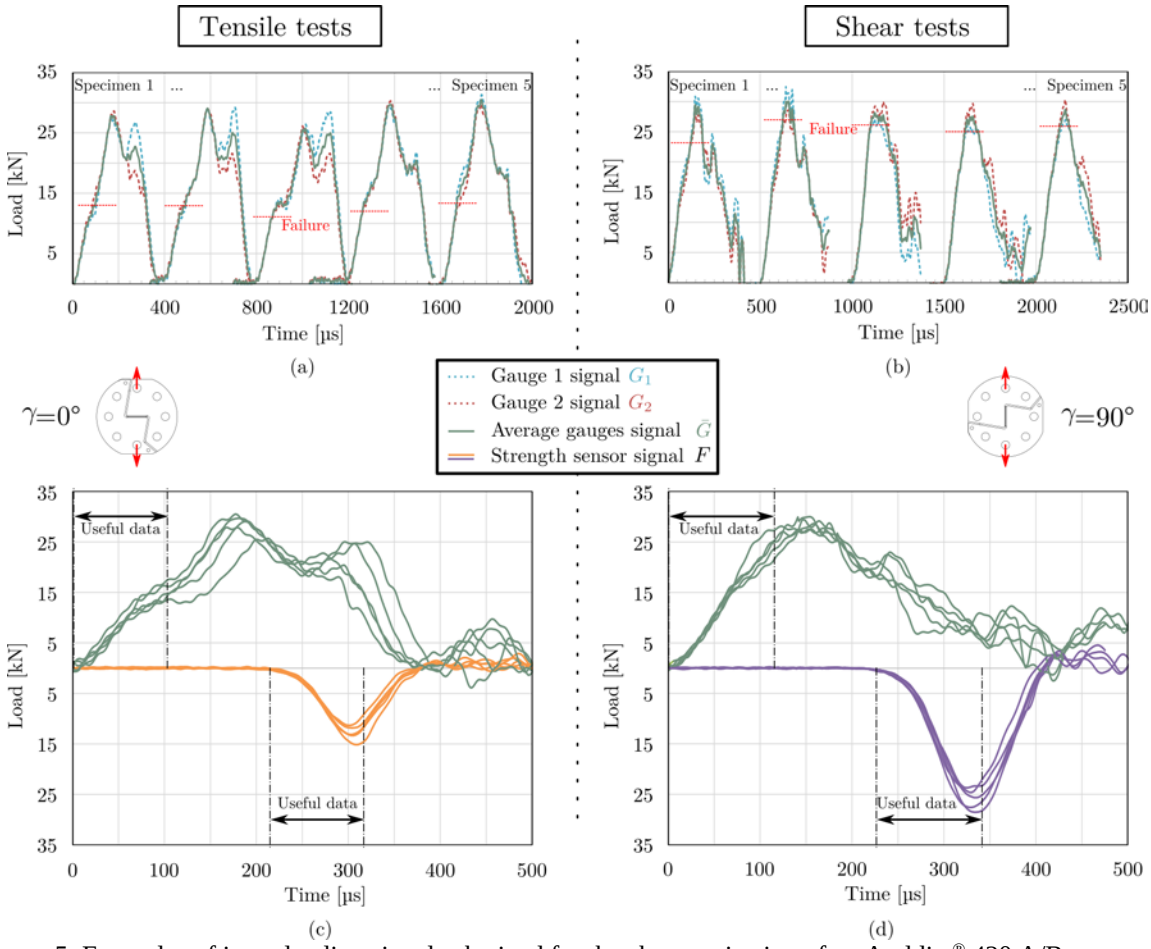

Figure 5: Examples of input loading signals obtained for the characterization of an Araldite® 420 A/B adhesive with $m = 100$ kg and $h = 0.5$ m. (a) Strain gauges signals extracted from tensile tests. (b) Strain gauges signals extracted from shear tests. (c) Strain gauges signals *vs*. load sensor signals extracted from tensile tests. (d) Strain gauges signals *vs*. load sensor signals extracted from shear tests.

At last, orange and purple signals plotted respectively in Figs. 5c & d correspond to the strength sensor signals associated to $\bar{G}$ ones. The part of the curves from the beginning of loading to failure of the sample is designated by a double arrow labelled "Useful data". First, Figs. 5a & b show that G_1, G_2 and $\overline{G}$ signals are always superimposed before the failure of the adhesive. That proves that the tensile rod is only subjected to a tensile loading (*i.e.* there is no bending). Secondly, it can be seen from Figs. 5a-d that for the same boundary conditions, input signals are repeatable and allow to obtain the failure of the adhesive on the first wave front. Thirdly, strain gauges signals and their associated load sensors signals plotted in Figs. 5c & d clearly show monotonic increases of the strength before the failure. Observations made from these two configurations can be extended to the other cases, for different adhesives and initial test conditions enabling to validate the test rig.

4. Post processing methods

4.1. Strain extraction

In order to extract strain components in the adhesive during the test, a method coupling the Digital Image Correlation (DIC) technic and the formulation of a finite element is used [14].

During the test, a high speed camera (see Fig. 4e for the location) records a 30×43 mm area @ 100 kHz containing the adhesive joint and the two substrates. In order to follow the

displacement of each substrate, a speckle pattern is painted on the surface of the substrates. After the test, a first image correlation algorithm allows to extract two displacement fields (*i.e.* one/substrate). A second algorithm, based on a minimization problem by least squares, is then used in order to determine the average rigid body motion of each of the two substrates from the previously extracted fields [17]. The rigid body motions are then used to compute an estimate of the displacement of the corners of the adhesive. The use of the usual shape functions of a Q4 four nodes finite element enables the computation of a strain field ε in the adhesive and so, on its average components of interest ε_{yy} and ε_{xy}.

4.2. Stress extraction

The stress extraction uses the load measures @ 1 MHz carried out by the load cell fixed above the test specimen (see Figs. 4d & e for the location). It was numerically demonstrated in [14] that during a test, there is no significant inertial effect induced by the substrate. Thereby, the force seen by the load cell is representative of the force seen by the adhesive at a small temporal time offset $\Delta t \approx 10$ µs (depends of the configuration γ) which corresponds to the time needed by the stress wave to go from the adhesive to the load cell. At last, average components of the stress tensor σ_{yy} and σ_{xy} are calculated by dividing the normal and tangential components of the force vector by the area of the adhesive.

4.3. Strain rate extraction

The strain rate extraction method choice is crucial since it connects the mechanical behaviour of the adhesive to a loading case. Two main methods can be used to identify this physical quantity: (1) via a theoretical calculation and/or (2) an experimental approach.

In the first case, an estimation of the strain rate is calculated according to the geometry of the adhesive and loading conditions. Following this theoretical approach, it is considered that the loading velocity of the adhesive is equal to the "set velocity" (*i.e.* to the crosshead velocity for tensile machine tests or to the impact velocity for drop weight tests). This assumption is strong in the sense that it does not take into account the properties of the adhesive and of the elements which are around. This generally results in an overestimation of the strain rate.

The experimental approach used for this study consists to recover the time derivative of the measured strain. The extracted value then corresponds to the strain rate actually seen by the adhesive. Figure 6a presents an example of a stress-strain curve extracted in the tangential direction from a shear test on a Betamate™ 1496V adhesive (*i.e.* $\gamma = 90°$). The test was carried out under quasistatic assumptions, on a tensile machine with an imposed crosshead velocity of $v = 0.5$ mm.min^{-1}. Figure 6b presents the time evolution of ε_{xy} associated to the same test.

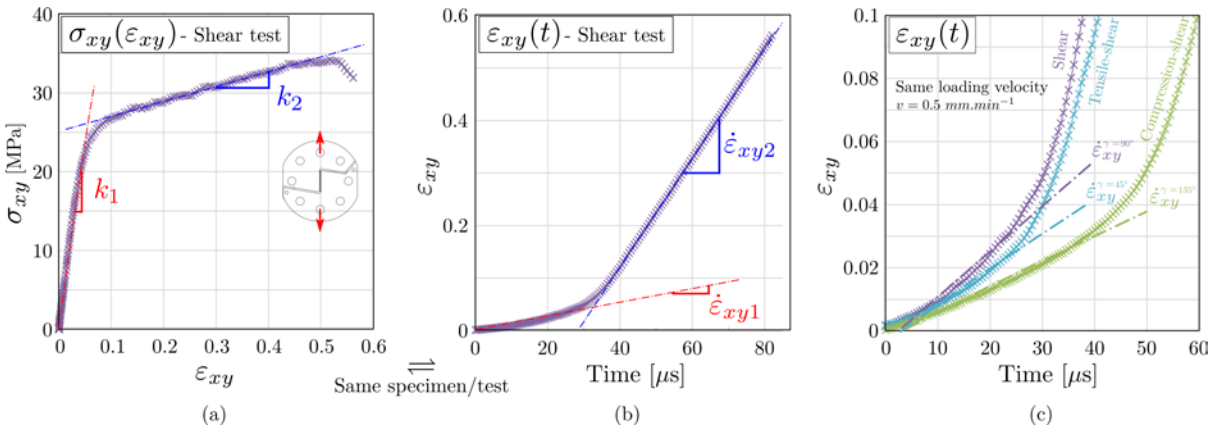

Figure 6: Strain rate extraction under quasistatic assumptions ($v = 0.5$ mm.min^{-1}) on a Betamate™. 1496V adhesive. (a) $\sigma_{xy}(\varepsilon_{xy})$ curve from a shear test example. (b) Time evolution of ε_{xy} from (a) example. (c) Influence of the configuration γ on the strain rate for the same input crosshead velocity.

On the latter, it is shown that even if the input crosshead velocity v is constant, two strain rates, noted respectively $\dot{\varepsilon}_{xy1}$ & $\dot{\varepsilon}_{xy2}$, can be measured. These are respectively connected to the linear part and to the plastic flow of respective stiffness k_1 & k_2 of the $\sigma_{xy}(\varepsilon_{xy})$ curve plotted in Fig. 6a. At last, a parallel with a spring can be done to explain that the strain rate increase (from $\dot{\varepsilon}_{xy1}$ to $\dot{\varepsilon}_{xy2}$) is the consequence of a stiffness decrease ($k_1 \rightarrow k_2$) directly linked to the mechanical behaviour of the adhesive. For the remainder of the study, only strain rates associated to the first linear parts of stress-strain curves will be used.

Figure 6c presents three examples of time evolution of ε_{xy} extracted from a tensile shear (in blue), a shear (in purple, the same curve as in Fig. 6b) and a compression-shear (in green) tests on a Betamate™ 1496V adhesive. In order to compare the strain rate of each curve, a zoom is carried out on the "$\dot{\varepsilon}_{xy1}$ parts". In the same way than for Figs. 6a & b results, all tests were made with the same crosshead velocity $v = 0.5$ mm.min^{-1}. As it can be seen, the measured strain rates are different from one configuration to another even if the input velocity is identical. This can be explained by different overall specimen stiffnesses according to γ and can be demonstrated theoretically via a three springs in series system. In other words, this last observation shows that for the same input conditions (v for quasistatic tests, (m, h) for dynamic ones), different strain rates can be measured according to the specimen orientation γ.

The observations made in this subsection on some examples under quasistatic assumptions can be extended to all configurations and also for dynamic results.

5. Results

5.1. Adhesive under investigation and bonding process

Experimental results presented in this section were made using 7075-T651 aluminium alloy substrates (material with very high strength used for transport applications; measured Young's modulus, Poisson's ratio and yield strength following NF EN ISO 6892-1 [20]: $E_s = 73$ GPa, $\nu_s = 0.35$ and $\sigma_y = 530$ MPa) and a Dow® Betamate™ 1496V adhesive (Young's modulus, tensile strength and lap shear strength given by the manufacturer following NF EN ISO 527-1 and NF EN 1465 [21, 22, 23]: $E_a = 1.6$ GPa, $\sigma_{yy\,\max} = 32$ MPa and $\sigma_{xy\,\max} = 30$ MPa). The latter is a one component, epoxy based adhesive especially developed for the body shop. The choice of the material for the substrates is derived from the specimen design

and from the choice of the tested adhesive in order to have a low ratio $\beta = E_s/E_a$ and satisfactory adhesion conditions.

Before assembling the two substrates, the bonded surfaces are sandpapered down with a grade of 80, degrease with acetone and cleaned with dry air. After laying the adhesive, the two positioning screws are placed. Cotton swab and spatula are used to clean the edges and the beaks. The curing cycle followed for all the specimens is 30 minutes @ 180°C (10 min. rise + 20 min. cure).

5.2. Repeatability of the results

Two test campaigns were carried out: (1) under the crosshead of a 100 kN tensile testing machine Instron® 8862 to obtain low strain rates and (2) under the dynamic tensile testing device presented in section 3 to obtain high strain rates.

Under quasistatic assumptions, a minimum of four specimens have been tested for each of the four loading directions with a crosshead velocity of $v = 0.5\ \text{mm.min}^{-1}$. Stress *vs.* strain curves and associated strain *vs.* time curves are respectively plotted in Figs. 7a & b and Figs. 7c & d for tensile tests (Figs. 7a & c) and shear tests (Figs. 7b & d). The plots show a good repeatability of the results with standard deviations less than 6 % for the ultimate strengths and less than 10 % for the strain rates.

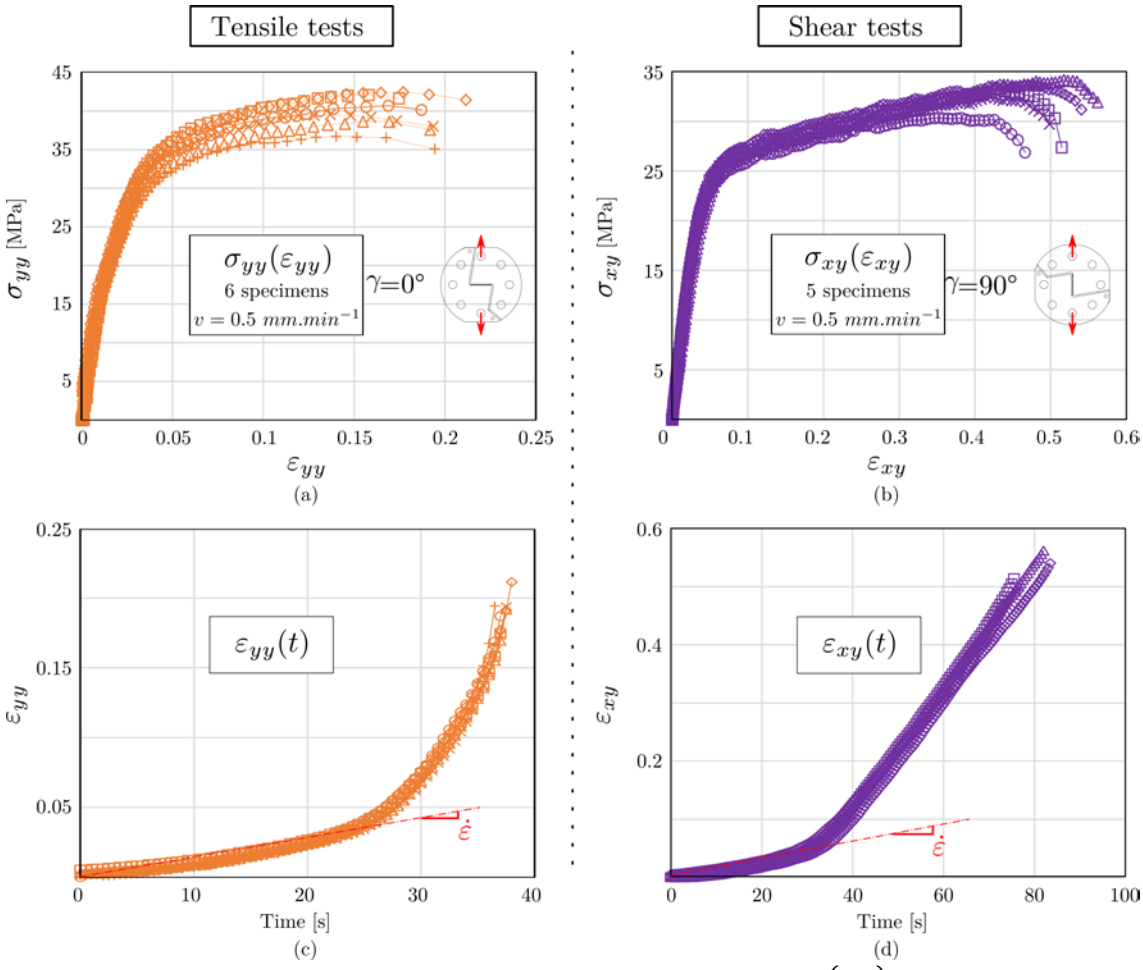

Figure 7: Repeatability of the results under quasistatic assumptions. (a) $\sigma_{yy}(\varepsilon_{yy})$ tensile tests results. (b) $\sigma_{xy}(\varepsilon_{xy})$ shear tests results. (c) $\sigma_{yy}(t)$ tensile tests results. (b) $\sigma_{xy}(t)$ shear tests results.

Under dynamic assumptions, a minimum of three specimen have been tested for each loading direction and each initial condition. Three falling heights $h = 0.1, 0.3$ & 0.5 m have thus been experimented with a $m = 200$ kg impactor. In the same way than for quasistatic results, stress *vs.* strain curves and associated strain *vs.* time curves are respectively plotted in Figs. 8a & b and Figs. 8c & d for tensile tests with $h = 0.1$ m (Figs. 8a & c) and shear tests with $h = 0.5$ m (Figs. 8b & d). These plots also show a good repeatability of the results with standard deviations less than 6 % for the ultimate strengths and less than 15 % for the strain rates.

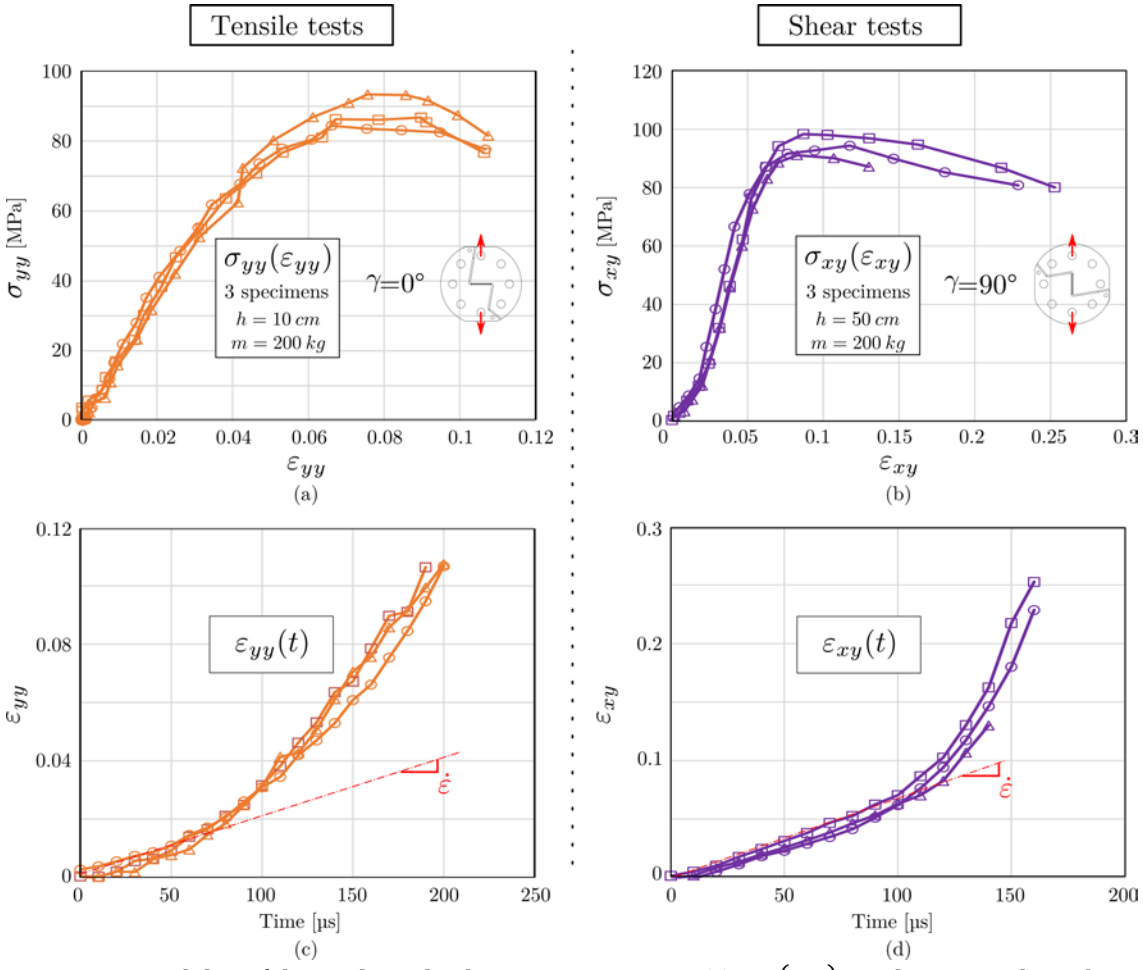

Figure 8: Repeatability of the results under dynamic assumptions. (a) $\sigma_{yy}(\varepsilon_{yy})$ tensile tests results with $h = 0.1$ m. (b) $\sigma_{xy}(\varepsilon_{xy})$ shear tests results with $h = 0.5$ m. (c) $\varepsilon_{yy}(t)$ tensile tests results with $h = 0.1$ m. (d) $\varepsilon_{xy}(t)$ shear tests results with $h = 0.5$ m.

5.3. Quasistatic vs. Dynamic stress-strain results

Stress-strain curves plotted in Fig. 9 correspond to examples extracted from each test series *i.e.* with different loading directions and initial conditions.

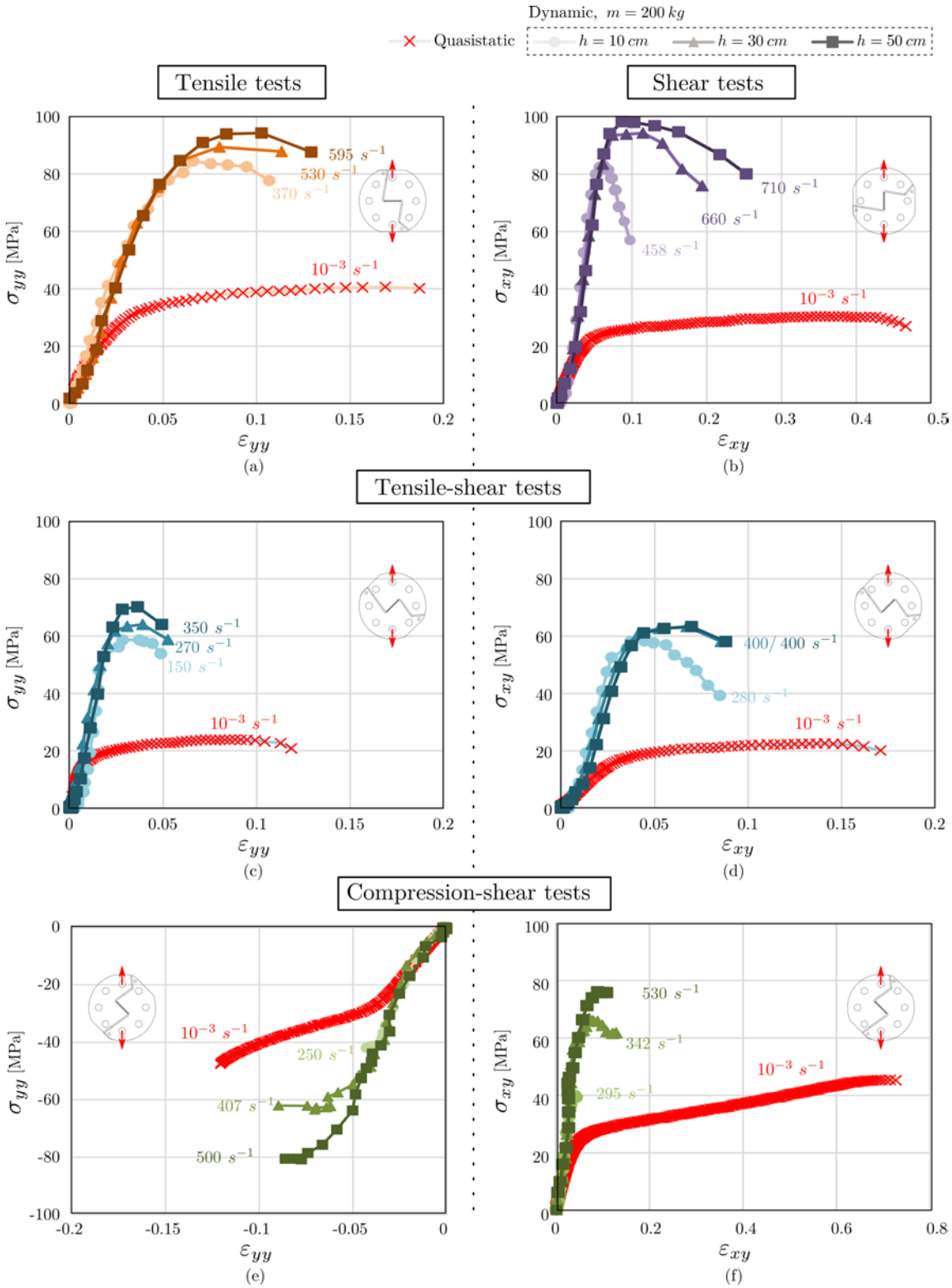

Figure 9: Quasistatic *vs.* dynamic stress-strain curves. (a) Tensile results. (b) Shear results. (c-d) Tensile-shear results. (e-f) Compression-shear results.

Thus, in Fig. 9a, the results coming from tensile tests in the normal direction, realized at several strain rates, are compared (Fig. 9b for shear tests in the tangential direction, Fig. 9c for tensile-shear tests in the normal direction, Fig. 9d for tensile-shear tests in the tangential

direction, Fig. 9e for compression-shear tests in the normal direction and Fig. 9f for compression-shear tests in the tangential direction). These results make it possible to draw up an initial assessment of the influence of the strain rate on the mechanical behaviour of the adhesive.

First, it can be noticed that the measured strain rates obtained by using the DTTD vary between 150 s^{-1} and 710 s^{-1} according to the specimen orientation and to the different initial conditions presented in subsection 5.2. Especially, an increase of the falling height and so of the impact velocity always leads to an increase of the strain rate.

A second observation is directly linked to the mechanical behaviour of the studied adhesive. This one is non-linear and clearly dependent of the strain rate which radically modifies its mechanical properties whatever is the loading case. In particular, it can be observed an increase of the stress limits and a decrease of the ultimate strains greater than 100 % between quasistatic results ($\dot{\varepsilon} \approx 10^{-3}\ s^{-1}$) and dynamic ones ($\dot{\varepsilon} \approx 10^{3}\ s^{-1}$).

These observations are in good agreement with the one made by May *et al.* [24] on butt joints made of Dow® Betamate™ 1496V loaded in traction with a fast driven servo-hydraulic testing machine at several strain rates. The stress *versus* strain curves are similar in terms of shapes and levels and the influence of the strain rate is confirmed.

In order to have a more synthetic and quantitative view of the impact of the strain rate, it is necessary to extract several mechanical properties from these results, according to $\dot{\varepsilon}$.

5.4. Stress and Strain envelopes

In this context, the evolution of six material parameters (that can be defined on the tensile stress-strain example presented in Fig. 10a) is studied according to the strain rate ($\dot{\varepsilon}$) These parameters are σ_e: the yield stress, $\sigma_{\max}$: the ultimate stress limit, ε_e: the yield strain limit (corresponding to σ_e), $\varepsilon_{\sigma_{\max}}$ the ultimate strain limit (corresponding to $\sigma_{\max}$), k_e: the elastic modulus and E: the total absorbed energy.

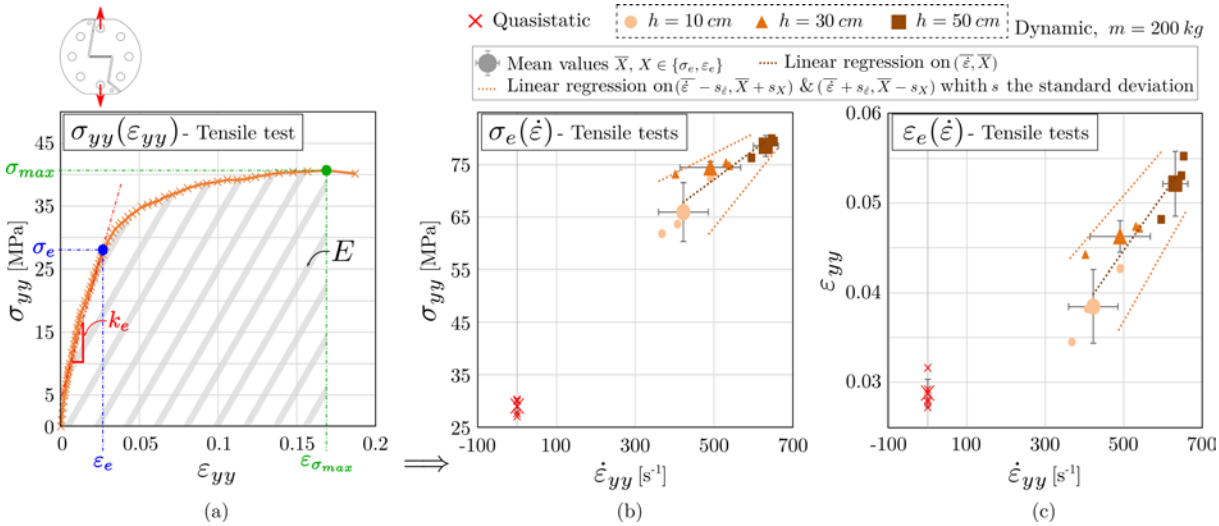

(a) (b) (c)

Figure 10: Envelopes extraction. (a) Locations of the studied parameters on a tensile stress-strain example curve $v = 0.5$ mm.min^{-1}. (b) $\sigma_e(\dot{\varepsilon})$ and (c) $\varepsilon_e(\dot{\varepsilon})$ results in the normal direction for tensile tests.

In this subsection, the stress and strain envelopes are studied. Because the strain rate varies from one loading case γ to another at iso initial conditions h and m (see subsection 4.3), it is necessary to interpolate the experimental results in order to be able to compare them at

iso $\dot{\varepsilon}$. To do this, a linear regression using a last squares method is realized on the mean values of coordinate $(\overline{\dot{\varepsilon}}, \overline{X})$, $X \in \{\sigma_e\ ,\ \sigma_{\max},\ \varepsilon_e\ ,\ \varepsilon_{\sigma_{\max}}\}$ from each series for the four loading cases γ and the two analysed directions x and y. Two others linear regression are realized on the extreme mean values of coordinates $(\overline{\dot{\varepsilon}} - \overline{s_{\dot{\varepsilon}}}, \overline{X} + s_X)$ and $(\overline{\dot{\varepsilon}} + s_{\dot{\varepsilon}}, \overline{X} - s_X)$ with s the standard deviation in order to respectively estimate the upper and lower bounds of the previous calculated values (three dotted lines in Figs. 10b & c).

Two examples are plotted in Figs. 10b & c which respectively correspond to the yield stress and strain evolutions in the normal direction according to the strain rate for tensile tests. All the evolutions of each parameter according to the strain rate for each loading case and direction are plotted in Appendix A.

From the regressions made upon the experimental results on the six defined parameters, it is then possible to obtained stress and strain response envelopes of the Betamate™ 1496V according to $\dot{\varepsilon}$. Figures. 11a, b, c & d respectively show the yield stress, ultimate stress, yield strain & ultimate strain envelopes. Normal components of the stress or strain tensor are defined on the abscissa axis and tangential components on the ordinate axis. On each graph the quasistatic envelope and the three dynamic envelopes obtained by approximation for $\dot{\varepsilon} = 300, 500\ \&\ 700\ \mathrm{s}^{-1}$ are plotted.

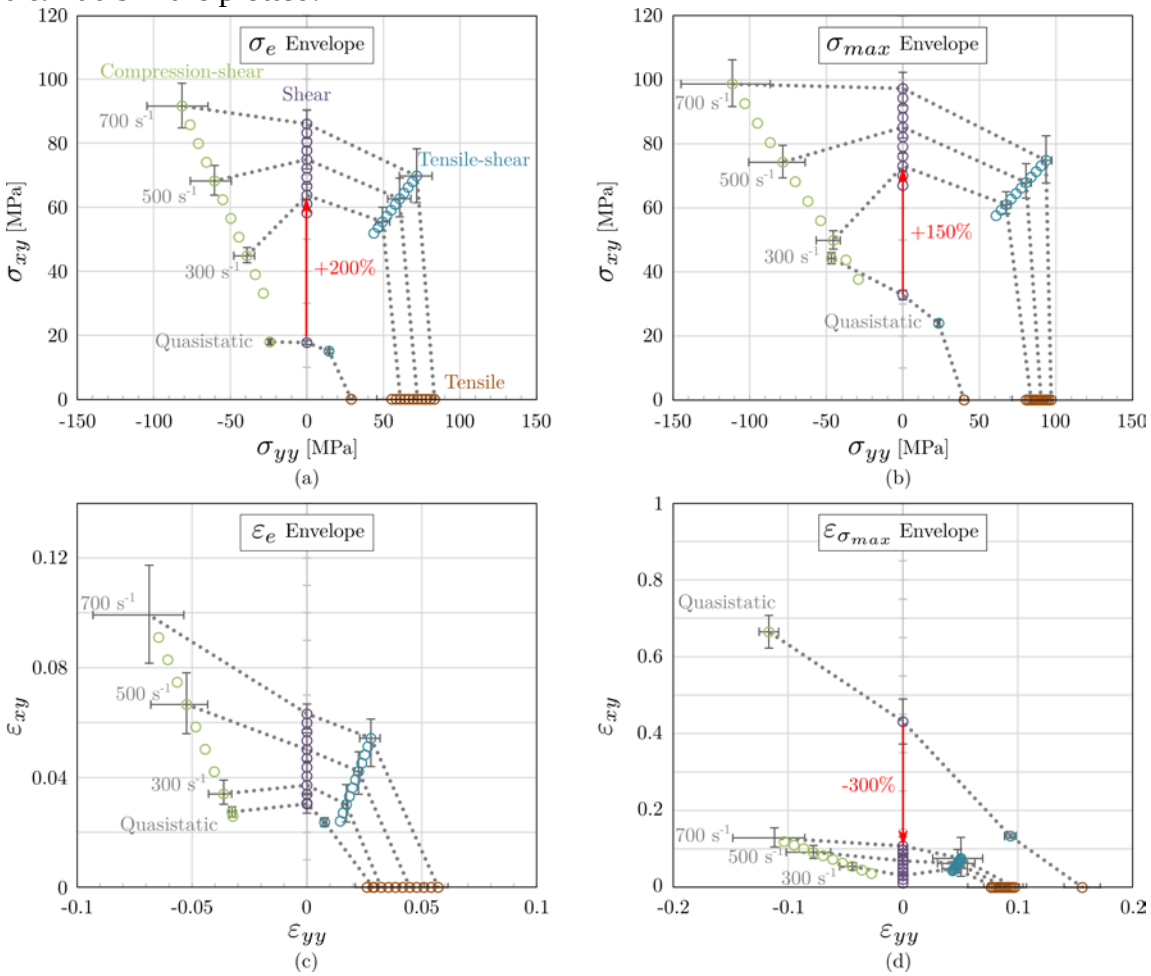

Figure 11: Response envelopes of the Betamate™. 1496V. (a) Yield stress σ_e envelope. (b) Ultimate stress $\sigma_{\max}$ envelope. (c) Yield strain ε_e envelope. (d) Ultimate strain $\varepsilon_{\sigma_{\max}}$ envelope.

Results from Fig. 11 confirm the first observations made in subsection 5.3. It can be noticed respective increases of the yield and ultimate stress limits of 200 % & 150 % for shear loadings and 80 % & 100 % for tensile loadings between quasistatic results ($\dot{\varepsilon} \approx 10^{-3}\ \mathrm{s}^{-1}$) and dynamic ones ($\dot{\varepsilon} = 300\ \mathrm{s}^{-1}$).

Regarding the yield strain envelope (see Fig. 11c), the $\sigma_e(\dot{\varepsilon})$ evolution induces a relative increase of the value of ε_e according to $\dot{\varepsilon}$. However, the ultimate strain envelope (see Fig. 11d) show a significant drop between quasistatic and dynamic results. Thus, it can be observed decreases of 300 % for shear loadings and 60 % for tensile loadings of the ultimate strain limits between $\dot{\varepsilon} = 10^{-3}\ \mathrm{s}^{-1}$ and $\dot{\varepsilon} = 700\ \mathrm{s}^{-1}$ results. Thereby, the adhesive behaviour becomes "more brittle" which could be a disadvantage for applications where the energy dissipation is wanted.

At last, σ_e, $\sigma_{\max}$ and ε_e envelopes also show gaps between $\dot{\varepsilon} = 300\ \mathrm{s}^{-1}$ and $\dot{\varepsilon} = 700\ \mathrm{s}^{-1}$. These are also larger for the tangential components (around 50 %) than for the normal ones (around 30 %) of the stress/strain tensors. These latter observations are not true for $\varepsilon_{\sigma_{\max}}$ envelopes (see Fig. 11c) where the gaps between dynamic values are of the same order than the uncertainties.

5.5. Elastic moduli & Total absorbed energies

In the same way than for the results presented in subsection 5.4, the elastic moduli k_e and the total absorbed energies E are extracted for each test. The results are plotted in Figs. 12 & 13 according to $\dot{\varepsilon}$. In Figs. 12a & 13a the values coming from the tensile tests in the normal direction are plotted for several strain rates. Figures 12b & 13b do the same for shear tests in the tangential direction, Figs. 12c & 13c and 12d & 13d are for tensile-shear tests in the normal and tangential directions whereas Figs. 12e & 13e and 12f & 13f stand for compression-shear tests in the normal and tangential directions.

It can be seen that for the initial conditions investigated under the drop tower, extracted values of k_e and E for each loading case and studied component are relatively similar in dynamic. In other words, quasistatic and dynamic results form two distinct groups separated by a jump.

The results for the elastic moduli k_{e} show an increase of the values between quasistatic and dynamic tests whatever the loading orientation γ. As for the other material parameters, the dependency towards the strain rate is more marked for the tangential components (from 100 % to 180 % of increase) than for the normal ones (from 25 % to 65 % of increase).

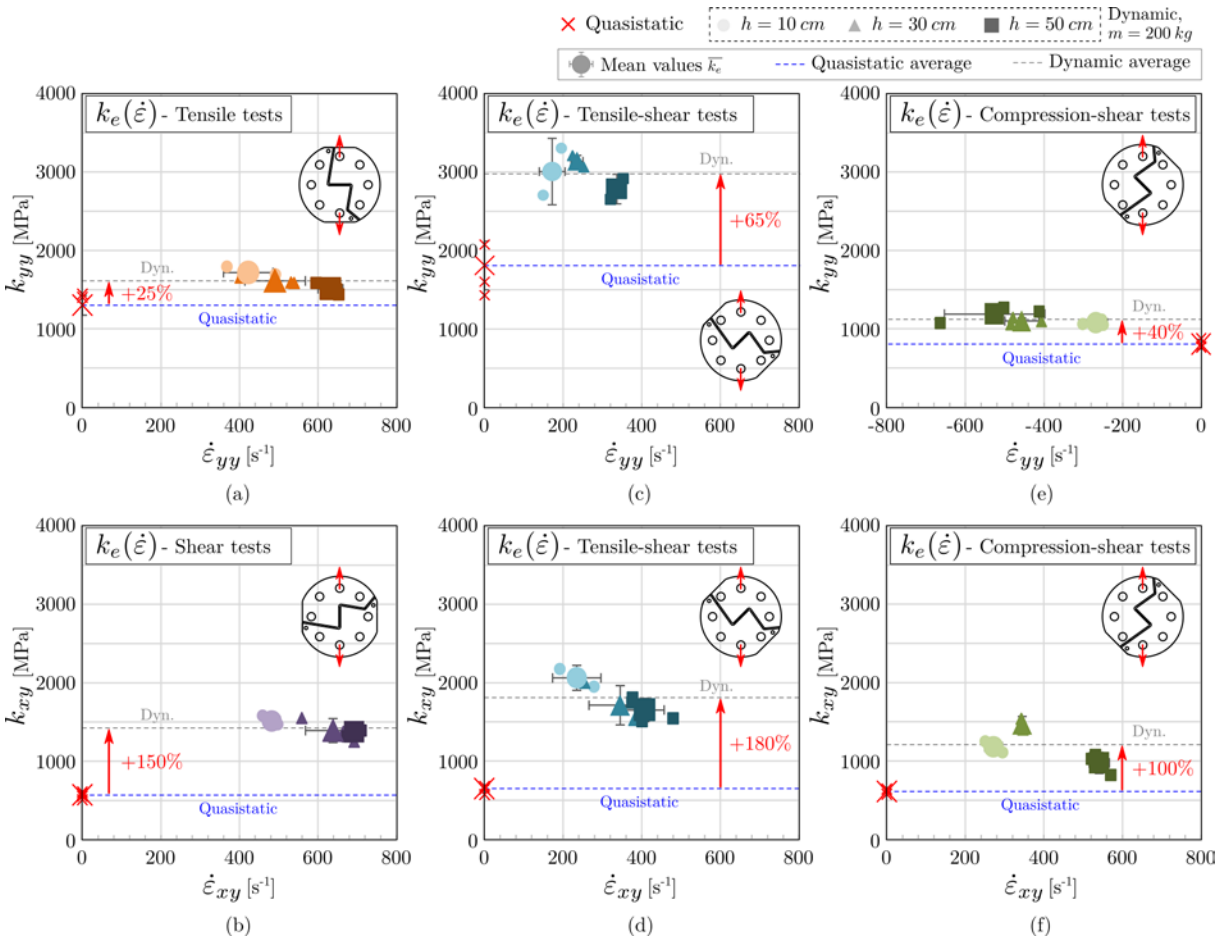

Figure 12: Elastic moduli k_e evolutions according to $\dot{\varepsilon}$. (a) Tensile results. (b) Shear results. (c-d) Tensile-shear results. (e-f) Compression-shear results.

By analysing the results about the total absorbed energies E (see Fig. 13, it can be seen that with the increase of the strain rate $\dot{\varepsilon}$ the energy absorbed tends to decrease, that is the adhesive tends to become more brittle. Indeed, if the small increase (7 % in the order of the measurement uncertainties) of the part related to the normal component of the energy dissipated in the tensile and tensile shear tests (Figs. 13a & c) is set aside, one can notice some significant loss of energy absorption capability of the adhesive, in particular in shear tests and compression shear tests (Figs. 13b & f) with respectively -59 % and -87 % upon the quasistatic capabilities. Once again, the strain rate influence is more important on the shear component than on the normal one.

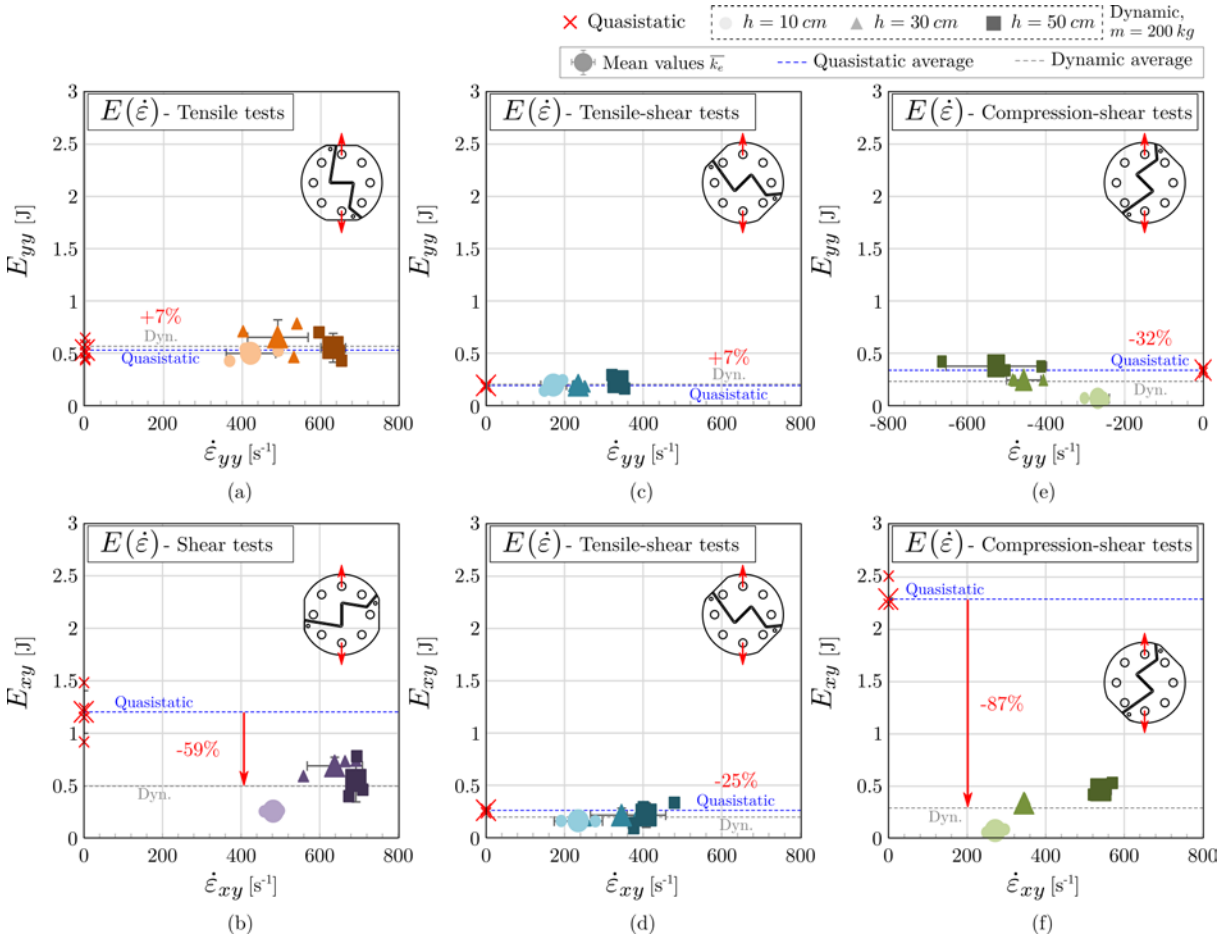

Figure 13: Total absorbed energies E evolutions according to $\dot{\varepsilon}$. (a) Tensile results. (b) Shear results. (c-d) Tensile-shear results. (e-f) Compression-shear results.

5.6. Fracture surfaces analysis

Examples of fracture surfaces pictures extracted from each tests series are presented in Fig. 14.

They show that for tensile, tensile-shear and shear solicitations, only cohesive failure were obtained. This is important to mention since this is a condition that is necessary to talk about material behaviour. In dynamic compression-shear tests, the lack of adhesive on some substrates is the result of the friction of each substrates after failure. From one loading case to another, different specific facies linked to different failure modes can be observed. However, results show identical facies between quasistatic and dynamic loadings which means that the strain rate has no influence on the failure modes.

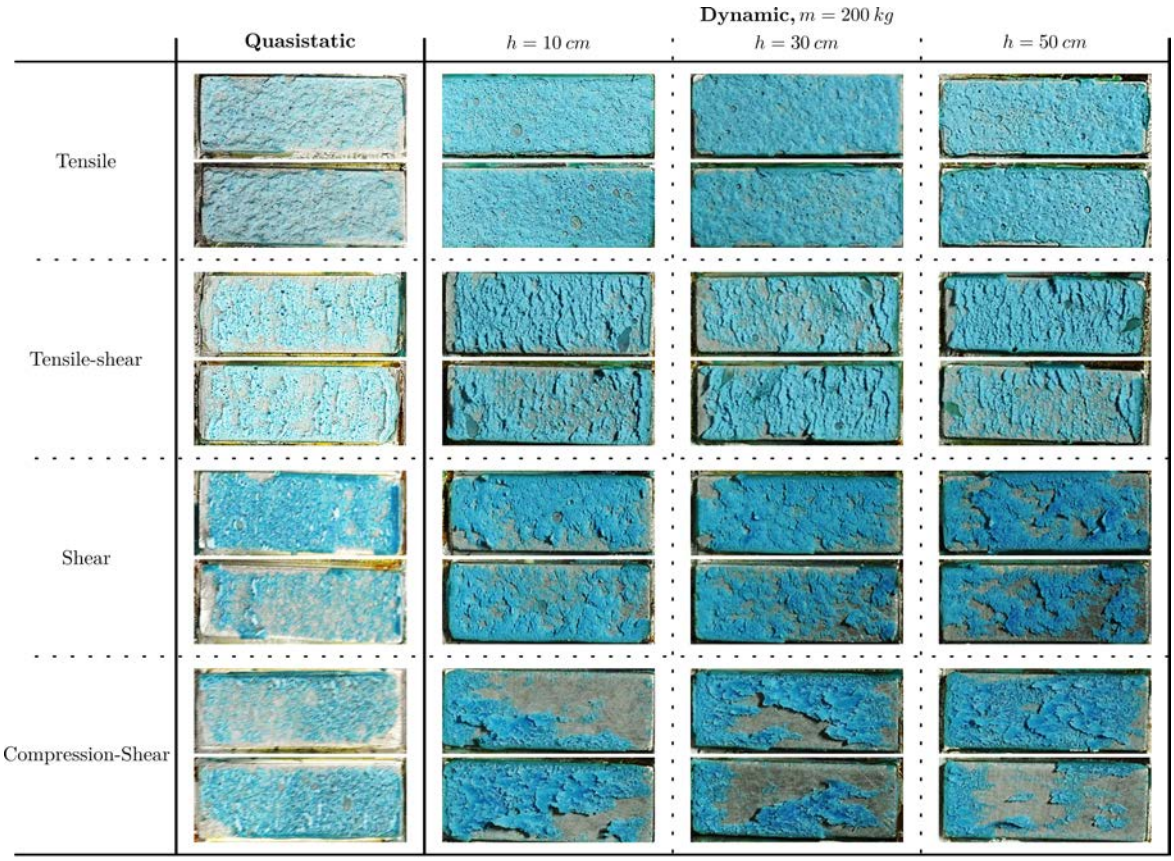

Figure 14: Examples of fracture surface from each initial condition and loading configuration.

6. Conclusions

This paper presents an original method dedicated to the dynamic characterization of structural adhesives under dynamic assumptions.

The tests relies on the use of a modified Arcan specimen corresponding to an evolution of the Tensile/Compression-Shear (TCS) Arcan developed by Créac'hcadec *et al.* [15]. This specimen is designed for dynamic loads and allows to test an adhesive under various loading directions and so to obtain its mechanical response envelope. The contribution of the substrates properties and of filleted "beaks" near the free edges of the adhesive ensures a quasi-homogeneous stress distribution along the overlap and minimizes the well known "edge effects".

A dynamic tensile testing device has been developed in order to set in motion the specimen at high rate velocity. This apparatus is positioned under a drop weight tower and transforms the kinetic energy stored by a falling impactor in a tensile loading. Its design is based on two main specifications allowing to obtain a qualitatively efficient test. For this purpose, it uses the modularity of the drop weight tower and particularly the ability to use a heavy impactor to produce a time and spatial stable loading of the adhesive as it was shown in [14].

This experimental assembly associated with the Arcan specimen were used for the characterization of a Dow® Betamate™ 1496V adhesive. Extracted results from this campaign are numerous, relevant & repeatable. The mechanical behaviour of the adhesive clearly depends of the strain rate which radically modifies its mechanical properties in terms of stress and strain limits.

These different results show the appropriateness of the development of this characterization test. Among other things, extracted mechanical response envelopes could be used for finite element modelling purposes or the development of adhesive formulations for application purposes.

From this study two perspectives should be investigated: (1) the validation of this testing device through the characterization of frequently used industrial adhesives under dynamic loadings; (2) the implementation of obtained results in a finite element model and the development of behaviour laws.

Acknowledgements

The authors acknowledge G. Cohen, P. Gilles & P. A. Rey from the Surfaces, Machining, Materials and Tools group of the Clement Ader Institute for their invaluable help on the manufacturing of Arcan specimens and F. Gilbert & D. Jacquet from ArcelorMittal, Montataire (France), for their financial support.

References

[1] I. Tawk, J. Aubry, P. Navarro, J. F. Ferrero, S. Marguet, S. Rivallant, S. Lemaire, P. Rauch, Study of impact on helicopter blade, Engineering Failure Analysis 24 (2012) 38–45.

[2] Standard test method for impact strength of adhesive bonds, ASTM D950-03.

[3] Adhesives - determination of dynamic resistance to cleavage of high-strength adhesive bonds under impact conditions - wedge impact adhesive, ISO 11343:2003.

[4] R. D. Adams, J. A. Harris, A critical assessment of the block impact test for measuring the impact strength of adhesive bonds, International Journal of Adhesion and Adhesives 16 (2) (1996) 61–71.

[5] R. Avendaño, R. J. C. Carbas, E. A. S. Marques, L. F. M. da Silva, A. A. Fernandes, Effect of temperature and strain rate on single lap joints with dissimilar lightweight adherends bonded with an acrylic adhesive, Composite Structures 152 (2016) 34–44.

[6] C. Sato, K. Ikegami, Strength of Adhesively-Bonded Butt Joints of Tubes Subjected to Combined High-Rate Loads, The Journal of Adhesion 70 (1-2) (1999) 57–73.

[7] Z. Jia, D. Hui, G. Yuan, J. Lair, K.-t. Lau, F. Xu, Mechanical properties of an epoxy-based adhesive under high strain rate loadings at low temperature environment, Composites Part B: Engineering 105 (2016) 132–137.

[8] P. C. Sato, Design for Impact Loads, in: L. F. M. da Silva, A. Öchsner, R. D. Adams (Eds.), Handbook of Adhesion Technology, Springer Berlin Heidelberg, 2011, pp. 743–763.

[9] J. E. Field, S. M. Walley, W. G. Proud, H. T. Goldrein, C. R. Siviour, Review of experimental techniques for high rate deformation and shock studies, International Journal of Impact Engineering 30 (7) (2004) 725–775.

[10] A. M. S. Hamouda, M. S. J. Hashmi, Testing of composite materials at high rates of strain: advances and challenges, Journal of Materials Processing Technology 77 (13) (1998) 327–336.

[11] P. L. Goglio, Impact Tests, in: L. F. M. da Silva, A. Öchsner, R. D. Adams (Eds.), Handbook of Adhesion Technology, Springer Berlin Heidelberg, 2011, pp. 503–532.

[12] L. F. M. da Silva, R. D. Adams, B. R. K. Blackman, L. Goglio, M. Peroni, C. Sato, K. Dilger, M. Frauenhofer, S. Kreling, Higher Rate and Impact Tests, in: L. F. M. d. Silva, D. A. Dillard, B. Blackman, R. D. Adams (Eds.), Testing Adhesive Joints, Wiley-VCH Verlag GmbH & Co. KGaA, 2012, pp. 273–317.

[13] B. Valès, S. Marguet, R. Créac'hcadec, L. Sohier, J.-F. Ferrero, P. Navarro, Numerical study of the local behaviour of adhesive bonds under dynamic loading, Journal of adhesion science and technology 30 (12) (2016) 1319–1339.

[14] B. Valès, S. Marguet, R. Créac'hcadec, L. Sohier, J.-F. Ferrero, P. Navarro, Experimental & numerical study of the tensile/compression-shear Arcan test under dynamic loading, International Journal of Adhesion and Adhesives 78 (2017) 135–147.

[15] R. Créac'hcadec, L. Sohier, C. Cellard, B. Gineste, A stress concentration-free bonded arcan tensile compression shear test specimen for the evaluation of adhesive mechanical response, International Journal of Adhesion and Adhesives 61 (2015) 81–92.

[16] L. Arcan, M. Arcan, L. Daniel, Sem fractography of pure and mixed mode interlaminar fracture in graphite/epoxy composites, ASTM Technical Publication, Philadelphia 948 (1987) 41–67.

[17] J.Y. Cognard, P. Davies, B. Gineste, L. Sohier, Development of an improved adhesive test method for composite assembly design, Composite Science and Technology 65 (2005) 359–368.

[18] J.-Y. Cognard, P. Davies, L. Sohier, R. Créac'hcadec, A study of the non-linear behaviour of adhesively-bonded composite assemblies, Composite Structures 76 (2006) 34–46.

[19] A. Beevers, M. D. Ellis, Impact behaviour of bonded mild steel lap joints, International Journal of Adhesion and Adhesives 4 (1) (1984) 13–16.

[20] Metallic materials - tensile testing part 1: Method of test at room temperature, NF EN ISO 6892-1.

[21] Dow® Automotive, Dow® Technical Datasheet - Betamate™ 1496V (2016).

[22] Plastics - determination of tensile properties - part 1: general principles - plastiques, NF EN ISO 527-1.

[23] Adhesives - determination of tensile lap-shear strength of bonded assemblies, NF EN 1465.

[24] M. May, O. Hesebeck, S. Marzi, W. Bhme, J. Lienhard, S. Kilchert, M. Brede, S.

Hiermaier, Rate dependent behavior of crash-optimized adhesives experimental characterization, model development, and simulation, Engineering Fracture Mechanics 133(2015) 112–137.

Appendix A

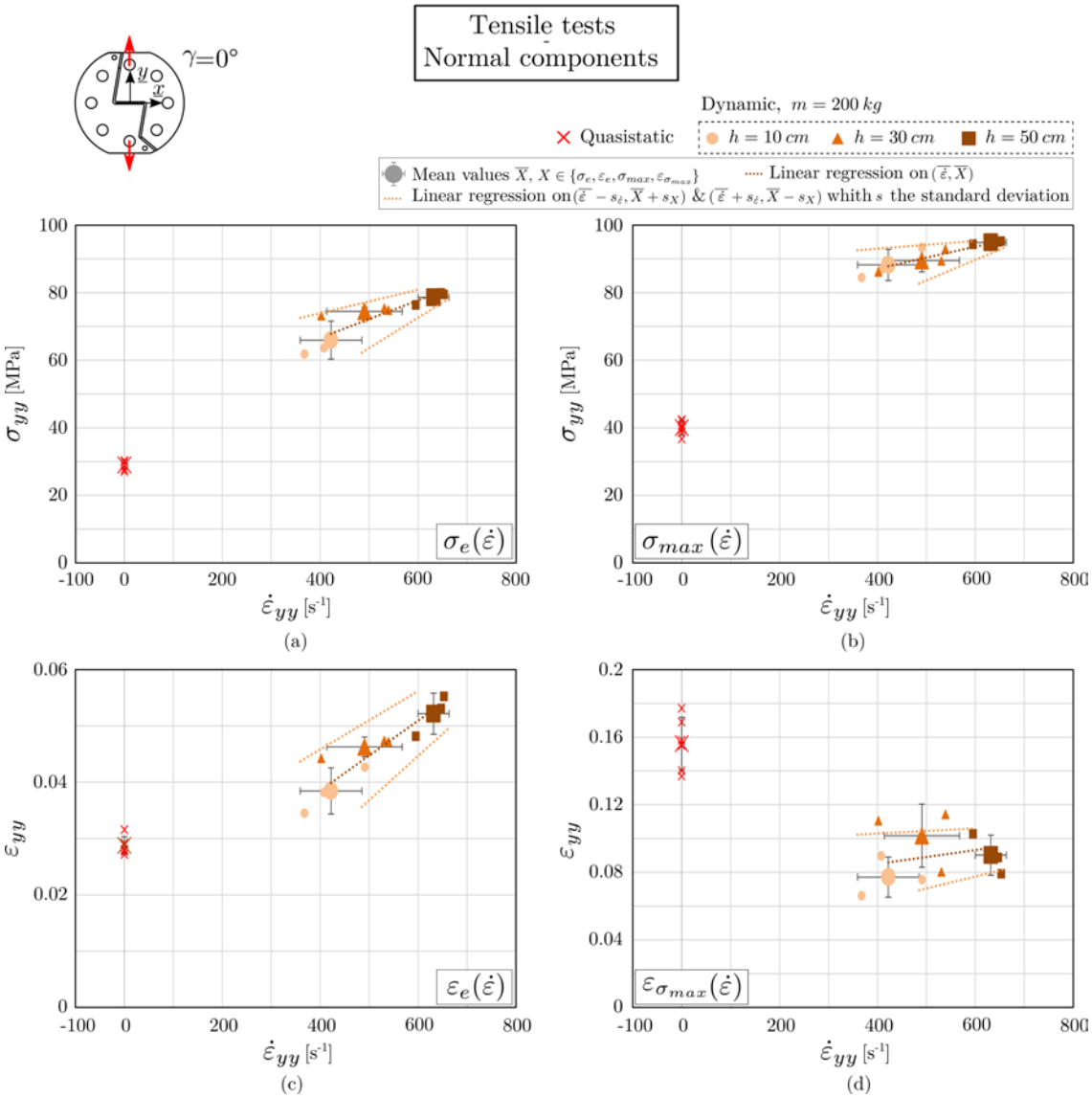

Figure A.1: Material parameters evolutions in the normal direction according to the strain rate for tensile tests. (a) $\sigma_e(\dot{\varepsilon})$ results. (b) $\sigma_{\max}(\dot{\varepsilon})$ results. (c) $\varepsilon_e(\dot{\varepsilon})$ results. (d) $\varepsilon_{\sigma_{\max}}(\dot{\varepsilon})$ results.

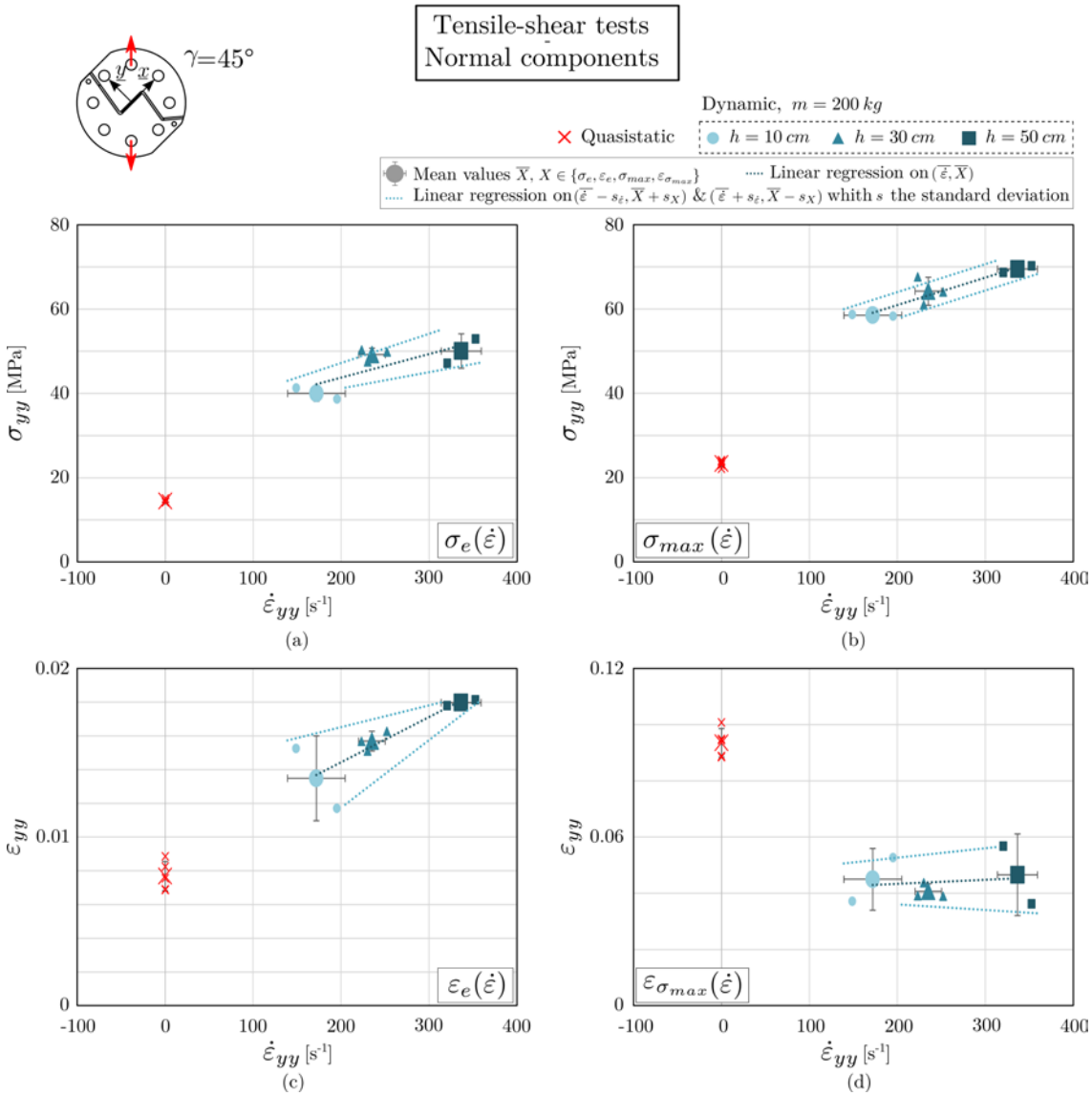

Figure A.2: Material parameters evolutions in the normal direction according to the strain rate for tensile-shear tests. (a) $\sigma_e(\dot{\varepsilon})$ results. (b) $\sigma_{\max}(\dot{\varepsilon})$ results. (c) $\varepsilon_e(\dot{\varepsilon})$ results. (d) $\varepsilon_{\sigma_{\max}}(\dot{\varepsilon})$ results.

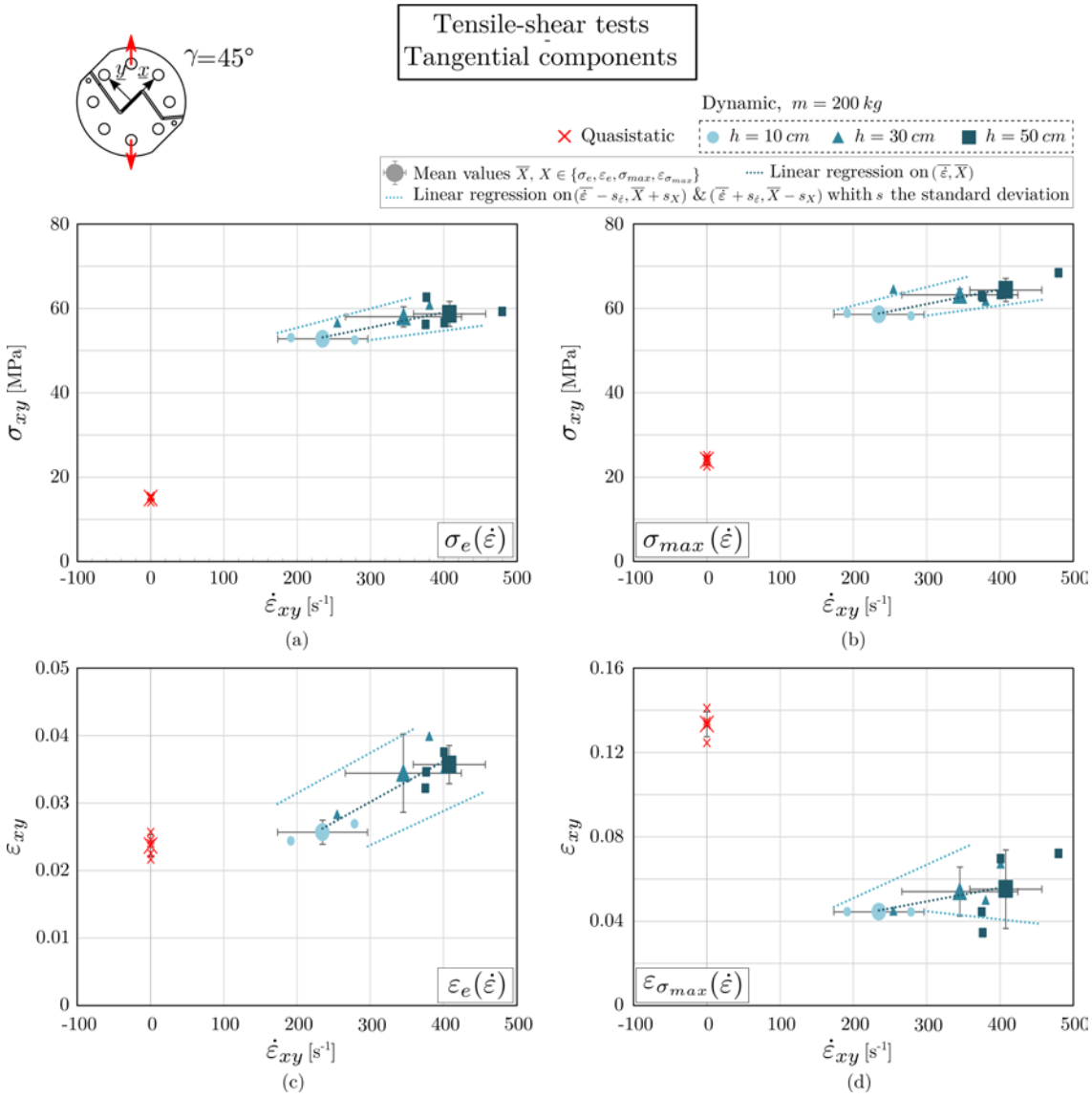

Figure A.3: Material parameters evolutions in the tangential direction according to the strain rate for tensile-shear tests. (a) $\sigma_e(\dot{\varepsilon})$ results. (b) $\sigma_{\max}(\dot{\varepsilon})$ results. (c) $\varepsilon_e(\dot{\varepsilon})$ results. (d) $\varepsilon_{\sigma_{\max}}(\dot{\varepsilon})$ results.

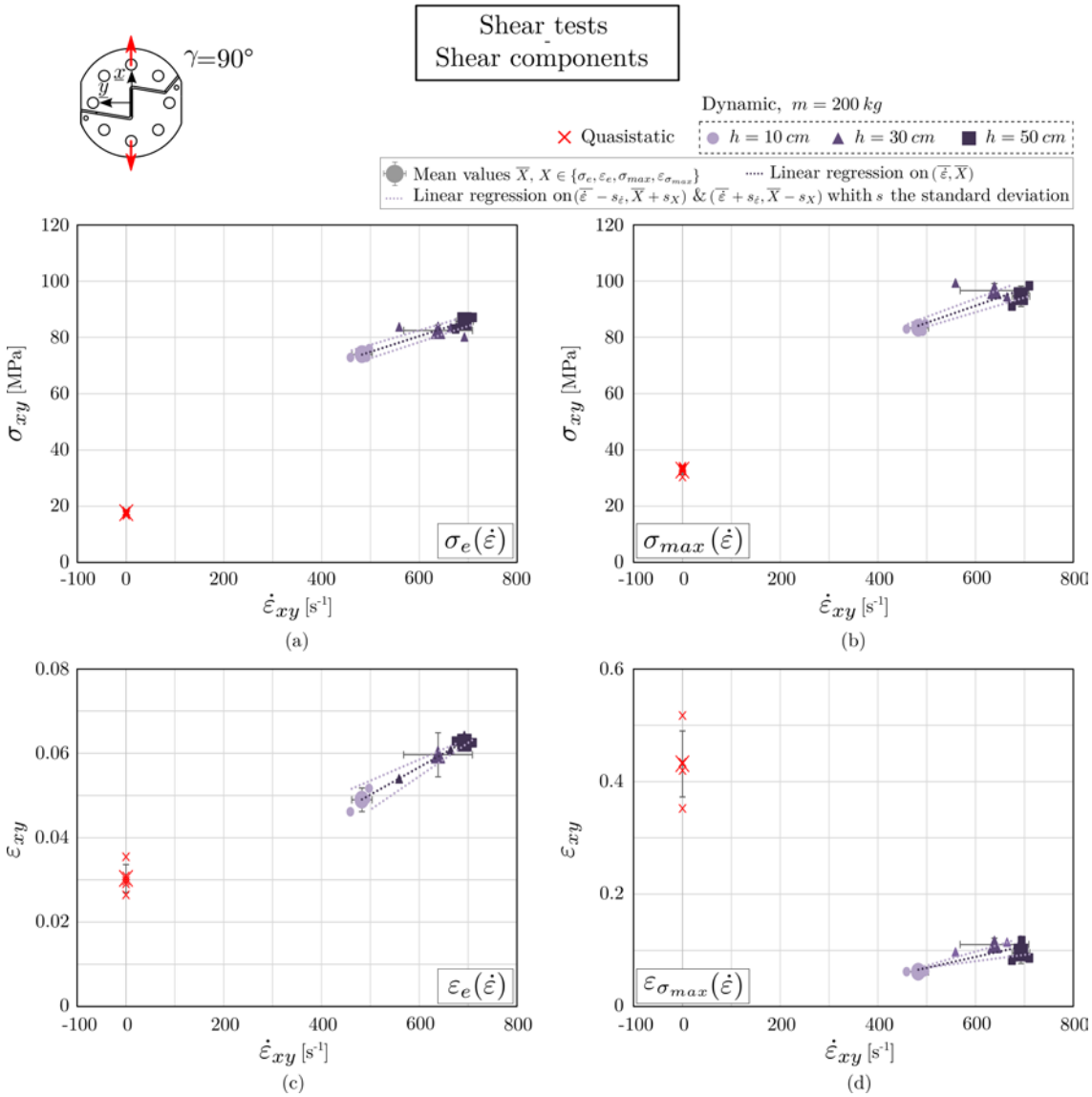

Figure A.4: Material parameters evolutions in the tangential direction according to the strain rate for shear tests.

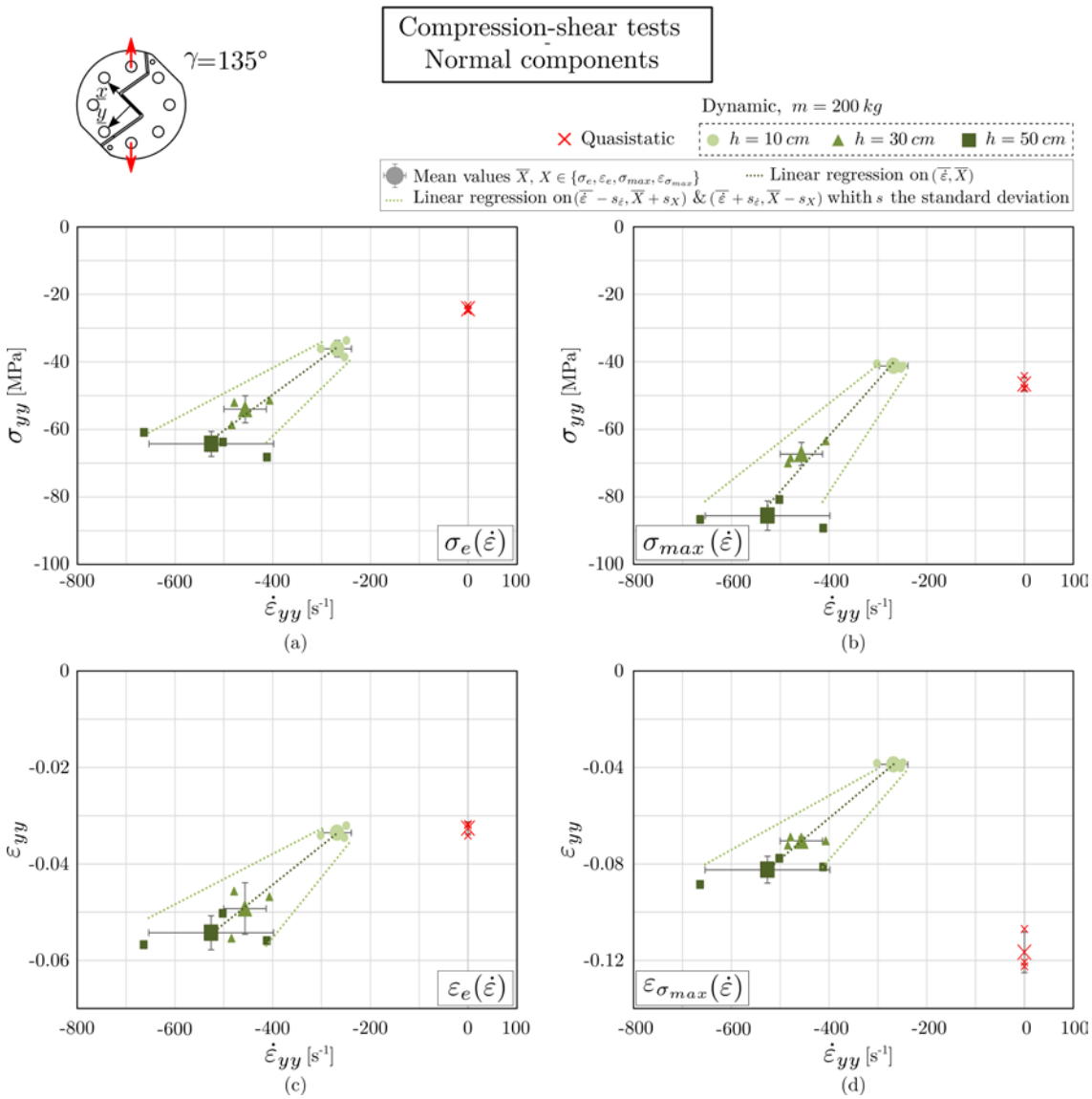

Figure A.5: Material parameters evolutions in the normal direction according to the strain rate for compression-shear tests. (a) $\sigma_e(\dot{\varepsilon})$ results. (b) $\sigma_{\max}(\dot{\varepsilon})$ results. (c) $\varepsilon_e(\dot{\varepsilon})$ results. (d) $\varepsilon_{\sigma_{\max}}(\dot{\varepsilon})$ results.

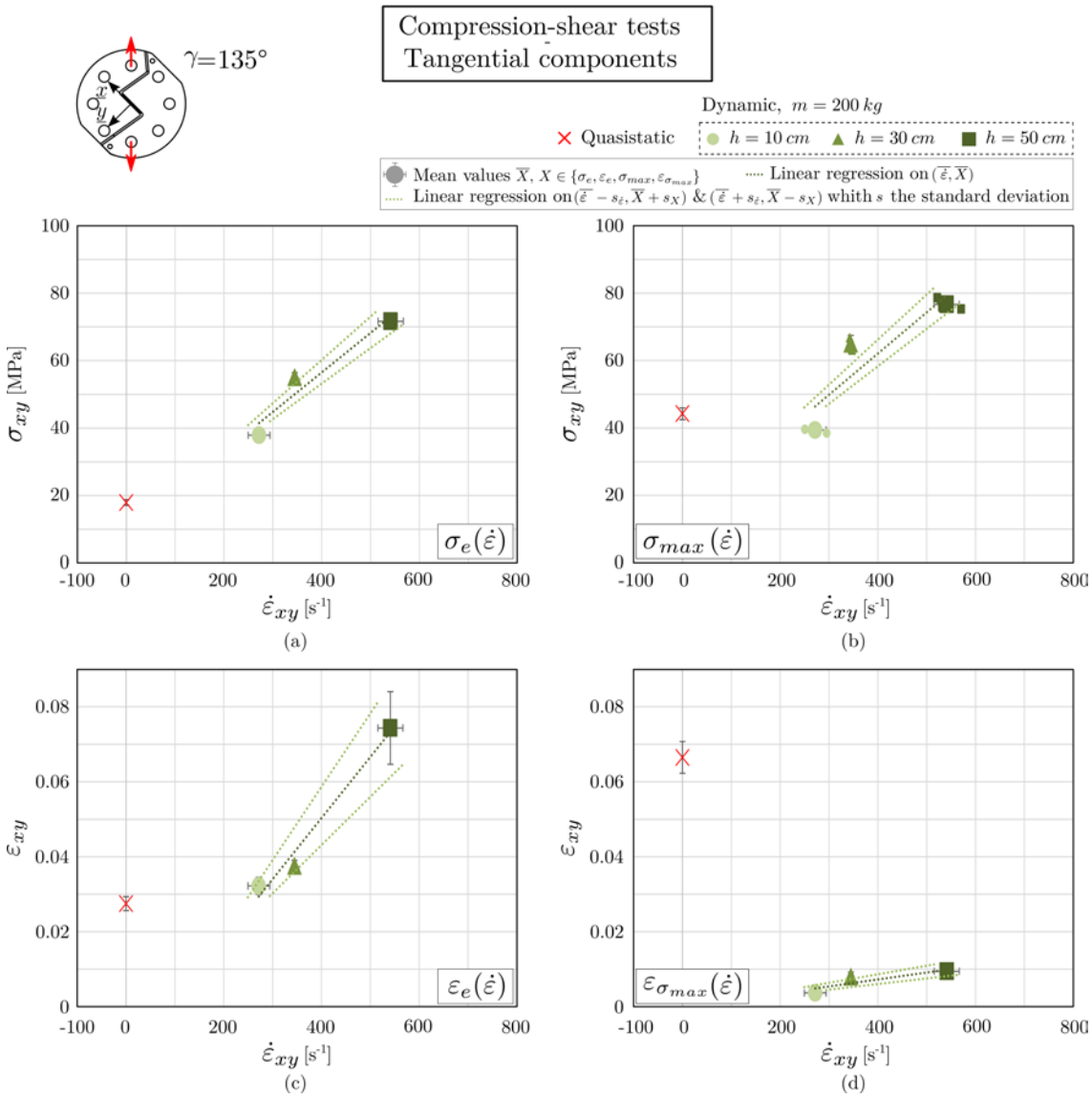

Figure A.6: Material parameters evolutions in the tangential direction according to the strain rate for compression-shear tests. (a) $\sigma_e(\dot{\varepsilon})$ results. (b) $\sigma_{\max}(\dot{\varepsilon})$ results. (c) $\varepsilon_e(\dot{\varepsilon})$ results. (d) $\varepsilon_{\sigma_{\max}}(\dot{\varepsilon})$ results.